

# Visual-auditory Extrinsic Contact Estimation

Xili Yi<sup>\*1</sup>, Jayjun Lee<sup>\*1</sup>, Nima Fazeli<sup>1</sup>

**Abstract**—Estimating contact locations between a grasped object and the environment is important for robust manipulation. In this paper, we present a visual-auditory method for extrinsic contact estimation, featuring a real-to-sim approach for auditory signals. Our method equips a robotic manipulator with contact microphones and speakers on its fingers, along with an externally mounted static camera providing a visual feed of the scene. As the robot manipulates objects, it detects contact events with surrounding surfaces using auditory feedback from the fingertips and visual feedback from the camera. A key feature of our approach is the transfer of auditory feedback into a simulated environment, where we learn a multimodal representation that is then applied to real world scenes without additional training. This zero-shot transfer is accurate and robust in estimating contact location and size, as demonstrated in our simulated and real world experiments in various cluttered environments. For more results and information, please visit [https://www.mmintlab.com/visual\\_audio\\_contact\\_estimation/](https://www.mmintlab.com/visual_audio_contact_estimation/).

## I. INTRODUCTION

Extrinsic contact estimation is a crucial capability for robots to accurately understand how grasped objects interact with their environment. Accurately estimating these contacts enables the robot to plan and control its actions effectively. Visual-based methods allow observation of the entire scene, but they often fall short in providing sufficient local information, particularly when contacts are occluded or within the resolution limits of the sensor. While tactile sensors or force torque sensors offer precise measurements of direct contact surfaces, they struggle to perceive indirect contacts, such as those between a tool and the environment. This challenge creates a sensing gap in extrinsic contact estimation. As illustrated in Fig. 1(d), distinguishing whether the grasped object is in contact when it is close to the table within the sensor’s resolution is difficult. Similarly, in Fig. 1(b), occlusions make it challenging to determine contact status.

To address this challenge, we propose a novel visual-auditory extrinsic contact estimation method. Our approach integrates global information from visual feedback with local information obtained through active audio sensing, as illustrated in Fig. 1(a). This enables the estimation of extrinsic contacts as masks in the 2D image plane of the camera, from which both the contact location and type can be inferred. Additionally, we introduce an audio-hallucination technique to overcome the difficulty of obtaining audio feedback in simulations. This technique involves injecting real world audio data into the simulation dataset with corresponding labels, thereby bridging the sim-to-real gap.

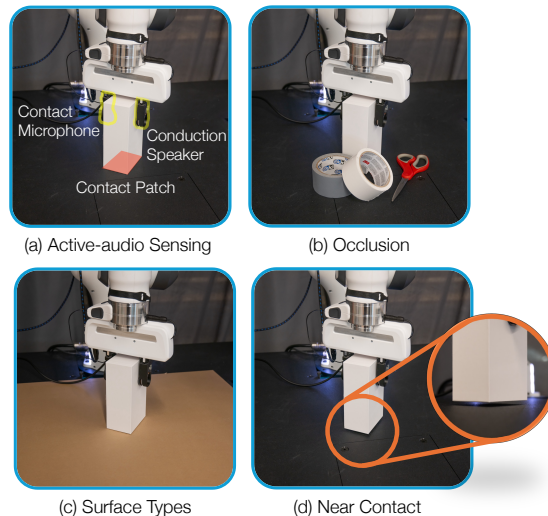


Fig. 1: (a) Our proposed fingers with an active conduction speaker and contact microphone emitting and receiving sound through the object. The absorption and reflection of the audio from the contact between the object and environment enables extrinsic contact estimation. Challenges include (b) where objects occlude the contact between the box and the table, (c) where a different surface type can change the acoustic feedback, and (d) estimating the object’s contact status purely from visual feedback for near-contact scenarios.

Our work builds upon and improves recent advancements in the field. A closely related study is *im2contact* [1], where a single RGB-D camera was used to learn a probability map of contact from cropped depth images, optical flow extracted from RGB, and proprioception. While this work demonstrates a promising direction to estimate contact locations in pixel space, two main issues persist. The first is that the existing method struggles with obtaining the location and shape of the contact patch in static scenes as it relies solely on the optical flow for extracting the temporal information of movement in the scene to infer contacts. Second, the existing approach is limited by occlusions and the resolution of the camera. By incorporating local active-audio information, our approach provides more comprehensive contact details, regardless of the contact and surface type, and in spite of heavy occlusion, addressing these limitations and enhancing the performance of extrinsic contact detection and the accuracy and robustness of contact geometry estimation.

## II. RELATED WORKS

In the field of manipulation, external contact sensing plays a crucial role. *Intrinsic contact*, which refers to the direct

<sup>\*</sup> Equal contribution

<sup>1</sup> Robotics Department, University of Michigan, USA <yixili, jayjun, nfz>@umich.edu

contact between the robot and the environment, has been well studied [2], [3], [4]. However, when manipulating tools, estimating *extrinsic contact*, such as sensing the contact between a tool held by the robot and the environment, becomes important. Sensing extrinsic contact is more challenging due to the indirect transmission of contact force/torque and the uncertainties in the object’s geometry, stiffness, and pose. [5] combines neural fields and vision-based tactile sensing to estimate the probability of extrinsic contacts between object and environment for any point on the object’s surface. Most studies rely on force/torque sensors or tactile sensors, which often involve strong assumptions or are limited to predefined contact configurations [6], [7], [8]. Some prior works require knowledge about the tool and the environment. For instance, [9] and the subsequent work [10] focused on estimating object pose and contact simultaneously. Additionally, data-driven methods have shown potential in estimating extrinsic contacts. [1] demonstrated that with visual data and robot proprioception, their model could predict the contact location in image space without assuming prior knowledge about the object and environment. [11] uses active tactile feedback to regulate a more consistent contact mode and make contact estimates for peg insertion tasks.

Audio is also a widely used modality in robotics as it can provide information on frequency components and vibrations due to its physical principles. Passive acoustic sensing directly uses sound waves from structural vibrations [12]. Some studies have modeled the sounds of object-surface interactions [13]. This approach is also commonly used in soft pneumatic actuators (SPAs) to sense state changes. Previous studies also showed that in end-to-end robot learning algorithms, including audio signals as input improved task performance [14], [15], [16]. Researchers also use active audio sensing methods to gain more information from the environment. Zöllner et al. detected contact by embedding a microphone into an SPA to measure the sound induced by contact [17]. Similarly, studies [18], [19], [20], [21] proposed embedding a microphone and a speaker in an SPA, playing sweeping sounds, and measuring changes from the microphone to sense deformation or contacts. Multimodal sensing with audio can be used for surface proximity detection with piezoelectric transducers for robot collision avoidance [22]. There are studies using active audio on rigid manipulator grippers to estimate grasp positions and for object recognition [23]. [24] uses a microphone at the gripper to receive audio feedback on contact events under partial observability. In this work, we utilize acoustic signals that transmit through objects with vision-based methods to estimate extrinsic contact using a model-free approach.

### III. VISUAL-AUDITORY CONTACT ESTIMATION

**Problem Statement:** Consider a robot holding an object and making contact with its environment as it moves. The goal of our method is to estimate the contact location and shape between the grasped object and environment. We assume no prior knowledge about the object or environment. We also assume objects are rigid or slightly deformable, i.e. erasers,

and the objects are all of graspable size. The inputs to our method are a depth map from a statically mounted camera, an optical flow image, fixed-length audio signals measured at gripper finger tip, and proprioceptive state of the robot.

**Method Overview:** We train a multimodal model that can predict contact probability maps over the scene given visual-auditory inputs. All the training data except for audio are synthetically generated in simulation where pre-recorded audio from the real world are injected. The model is then zero-shot transferred to the real world. The following sections, outline the data generation process, active-audio sensing, model architecture, and training unique to this problem.

#### A. Dataset Generation and Real-to-Sim Audio Hallucination

One main challenge in this task is to obtain a dataset with aligned vision, audio, and correct contact patch labels. From the real-world experiments, it is relatively easy to obtain the audio information along side with both depth maps and robot proprioception data. However, obtaining correct contact patch masks is not only hard but also inaccurate with human labels. This is because there is no direct way to observe the exact contact patch shape and size. Meanwhile in simulation, it is simple to generate a large dataset with both correct contact patch masks and labels. However, obtaining realistic audio signals from simulation remains a great challenge.

To overcome this challenge, we propose an audio hallucination technique. In the real-world, we collect audio signals ( $\mathbf{v}_t$ ) as the robot is grasping and moving various objects in the environment. During the robot motion, we record contact and contact geometry labels ( $\mathbf{g}_t$ ) from the set  $\{\text{free, point, line, patch}\}$ . We emphasize that we do not record locations or geometry, only simple to observe labels. Thus the audio labeled dataset is  $\mathcal{D}_{\text{audio}} = \{(\mathbf{v}_0, \mathbf{g}_0), \dots, (\mathbf{v}_n, \mathbf{g}_n)\}$ . Next, in simulation we create scenes with the same robot and table as well as a large distribution of objects that the robot can grasp and interact with. This distribution of objects is not the same as the real-world set. The simulator is able to render the visual scene as a depth map ( $\mathbf{d}_t$ ) and provides proprioception ( $\mathbf{p}_t$ ). We also take one depth map when the object is lifted without contact as a reference frame ( $\mathbf{r}_t$ ) of the grasped object. Although the simulator can generate optical flow images, we generate the optical flow ( $\mathbf{f}_t$ ) using an off-the-shelf RAFT model [25] to later facilitate sim-to-real transfer, where we use the same model to generate the optical flow images for the real world test data. We note that we generate optical flows only from depth maps to avoid the influence from shadows. Most importantly, the simulator also directly provides the contact geometry label and its corresponding shape ( $\mathbf{s}_t$ ) when contact occurs. At each contact event, we randomly select a sample of the real-world audio corresponding to the label provided by the simulator and create a labeled dataset of contacts  $\mathcal{D} = \{(\mathbf{O}_0, \mathbf{s}_0), \dots, (\mathbf{O}_m, \mathbf{s}_m)\}$  where the first element is the observation vector  $\mathbf{O}_i = (\mathbf{v}_i, \mathbf{d}_i, \mathbf{r}_i, \mathbf{f}_i, \mathbf{p}_i)$  and the second is the label.

The premise of our approach is that the audio signatures from specific contact geometry, while variable across specific

object interactions, share sufficient features that distinguish them from one another. Thus, a model trained on this dataset will learn to ignore the details of the audio signatures for specific objects and focus on acoustic features that correlate with contact geometry and mode.

### B. Active-Audio Sensing



Fig. 2: (1) A sweeping acoustic signal is generated from (2) using a conduction speaker, where (3) the sound propagates through the object and vibrates with any extrinsic contact it makes, which is received at (4) the contact microphone finger, and (5) the waveform is converted to a spectrogram.

Suppose that the robot is holding an object and dragging it across a surface. The physical interaction between the object and environment creates an audio signature that contains a wealth of information about the interaction including its location and speed. However, if the object is in a static contact with the environment, there will be no audio signals from the relative motion of the object, as audio signals require a source, from either motion or an active audio source. To generalize the robot’s perception capabilities to static scenes, we implement an *active-audio system* where one finger acts as an actuator and the other as a receiver, as shown in Fig. 2. With this approach, even without motion, we can detect audio differences as the environment absorbs or amplifies some of the acoustic energy upon contact.

The frequency characteristics of each object and contact vary depending on their physical properties, including stiffness and geometry. To comprehensively capture these properties, we use a sweeping sound as input to the object, as it contains all frequencies. We collect audio feedback from a microphone and then use Short-Time Fourier Transform (STFT) and scaling to generate a log-mel spectrogram using 64 mel frequency bins. In the spectrogram, shown in Fig. 2(c), the x-axis represents time, the y-axis represents frequency, and the color represents energy at that time and frequency. The frequency axis is non-linearly scaled to show more information in the lower frequency range, which typically contains more useful information. Given its ability to display both temporal and frequency information and their relationship, we choose this as the audio representation.

We fix the time horizon of each audio to one second, and output a sweeping sound to the object at the middle of that horizon (after 0.5 seconds), to cover the impulse responses across ranges of frequencies, while the first half does not generate the sound to record any audio feedback signal from the interaction with the environment.

### C. Simulation

We used Isaac Gym simulator [26] to replicate the real world scene for collecting training data. In each episode,

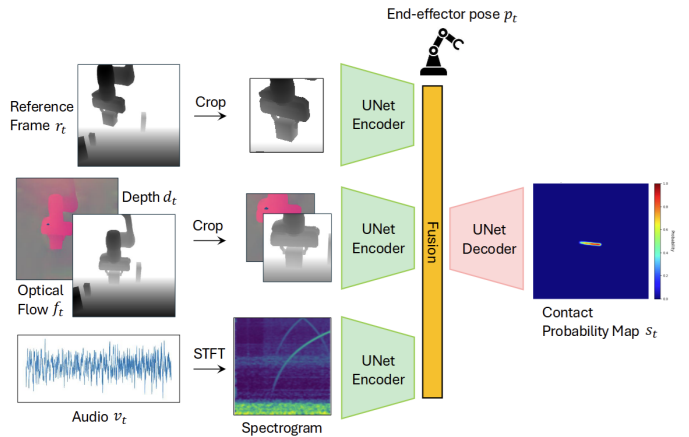


Fig. 3: Model architecture for visual-auditory extrinsic contact estimation. Inputs include a depth and optical flow from the current frame and a reference object image along with an audio feedback. The model outputs a probability map, which can be thresholded to obtain a contact mask prediction.

the robot grasps a random object and rotates to a random orientation, then lowers down to the tabletop, and starts sliding the object on the table. For each environment, we randomly select cubes with random size and objects from YCB dataset [27] that are smaller than 10cm in diameter. We obtain the contact points of the object and the environment, then project them back to the camera frame to obtain the contact masks. We also obtained a contact label from the size and shape of the contact patch, which are `[free, point, line, patch]`. With these labels, we randomly select real-world audio samples with the same labels and then pair with depth image. The training data contains 4100 episodes where each episode contains around 20 frames, which approximates to a total of 82k data sample.

### D. Model Architecture

For visual-auditory extrinsic contact estimation, our model architecture builds on the UNet architecture [28]. The model consists of three streams of UNet encoders, each processing different streams of data that are fused at the bottleneck. The main stream encodes a depth image and an optical flow image at the current frame, cropped around the projected End-Effector (EE) pixel coordinates and stacked along the channel dimension. The second stream encodes a cropped depth image of the object at a reference frame and the third stream encodes an image of a log-mel spectrogram from a 1s long audio waveform sampled at 44.1 kHz. All input images are of size  $256 \times 256$  and the 7DoF robot pose is fused at the bottleneck of the UNet. For every cropping operation, additional three channels are stacked for coordinate convolution [29] and providing the model with explicit information about the spatial position of each pixel within the cropped image and help the model maintain understanding of spatial relationships after cropping. The model output is the contact probability map that predicts the contact patch as a single channel mask image.

### E. Training Details

We train our model using the pixel-wise binary cross entropy (BCE) loss with logits using the ground-truth contact masks obtained from simulation with a batch size of 32 and a learning rate of  $5e-4$  for 5 epochs on 4 NVIDIA RTX A6000 GPU. One major challenge with extrinsic contact estimation is when the contact location of the grasped object is heavily visually occluded due to clutter. Prior work [1] has shown the efficacy of using image cropping, utilizing contact-free reference depth images of the grasped object, and optical flow for contact estimation. Cropping the input images of the task scene centered around the EE position, projected onto the pixel space, simplifies the learning problem by removing background distractions and with an improved focus on the tool-environment interaction. Providing a contact-free reference depth image of the object in the gripper also informs the model about the object geometry before the scene becomes cluttered. Moreover, visual ambiguities are present when differentiating an in-contact versus a near-contact state of the robot. This can be partially resolved by introducing the optical flow as an input to represent the temporal information of the robot motion. In addition to adopting these strategies, we further utilize the audio modality to acquire feedback from extrinsic contact and interaction with the environment from the sine sweep impulse response that can also provide the model with the temporal information about contact events and contact mode type.

## IV. EXPERIMENTS

To evaluate the performance of visual-auditory extrinsic contact estimation, particularly the role of acoustic signals from contact, we focus on the following. We examine whether active-audio signals provide useful information for detecting the extrinsic contact between the gripper-held object and the environment, such as a table, and for identifying the contact geometry. Then, we assess the effectiveness of real-to-sim data generation and investigate the importance of audio signals for sim-to-real generalization, including how well audio can complement vision, especially in scenarios with occlusion and when the object is near-contact.

### A. Experiment setup

Our real-world experiment setup consists of a Franka Emika Panda robot arm mounted to a table as well as the active-audio fingertips mounted on the gripper. Both the input and output audio signals from the fingers are routed to a computer through a Focusrite Scarlett 4i4 3rd Gen amplifier. We set a realsense cameras pointing to the table for collecting RGB-D images. We selected the following objects from the YCB dataset [27]: [spoon, big clamp, small clamp, Pringles, apple, lemon, orange, pear, screw driver, scissors, pods] in addition to a realsense box and a dustpan as test objects.

### B. Data Collection for Real World Audio

Active-audio fingertips are mounted onto the gripper, connected to the robot system. To generate sample audio for audio hallucination, we selected 6 objects [small box, big

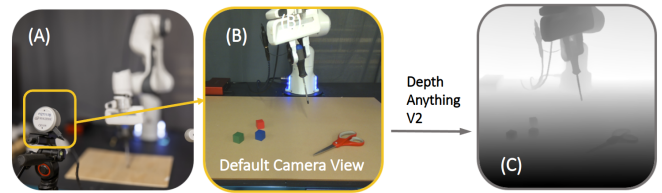


Fig. 4: (A) A realsense camera is used in the real world setup (B) to collect RGB images, and (C) Depth Anything V2 is used to generate artifact-free depth.

box, can, toy brick, clamp, potato chips tube] as test objects. As for the contact environment, we used our rough black plastic table top as the default contact surface.

To collect active audio feedback from different types of contact, we manually jog the robot to random orientation after the robot has grasped an object, and make contact with the environment. We store the pose as a reference pose, and label it with its corresponding contact geometry semantic label. Then with this reference pose, the robot randomly chooses motion in 2 dimensions: (1): [static, linear motion] and (2): [free space, contact with table]. During these motions, we capture active audio feedback from the scene. For each motion, we collect 1 second long single channel 44100 Hz audio from the robot’s gripper. During this step, all contact modes are possible. Each sample includes a sweeping sound ranging from 20 Hz to 20,000 Hz between 0.5 and 1.0 seconds of the recording. We also label each audio sample based on the robot’s motion and orientation to identify the contact geometry label. We collected 1000 audio samples with a variety of objects, contact shapes and contact modes.

### C. Data Collection for Real World Test Data

For real-world depth collection, we use a statically mounted front-view L515 Realsense camera, to collect their RGB images and use Depth Anything V2 [30] to generate hole-less depth maps. We use the same audio collection pipeline as in Section IV-B for collecting the test data.

The contact masks in the real world test dataset are annotated manually, with the help of RGB images collected along with the depth. We note that these masks are subject to the annotator’s subjective experience due to occlusion and the difficulty in directly observing ground truth contacts.

### D. Real World Test Scenarios

To evaluate the sim2real transfer of our models on the extrinsic contact estimation problem, we design the following real world test scenarios. These highlight the key challenges faced where the information of contact cannot be seen via vision as well as the significant sim2real gap.

- **S1**: Generalization to novel gripper-held object geometry.
- **S2**: Generalization to scene distractors.
- **S3**: Occlusion cases where the contact region is hidden.
- **S4**: Generalization to unseen table surface type.
- **S5**: Near contact cases that are not in contact.



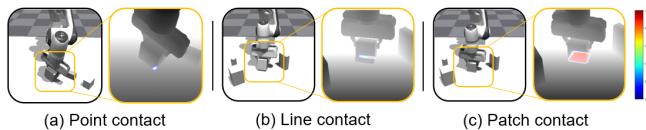


Fig. 5: Different contact modes covered in the simulation data. The cropped depth is centered around the projected pixel coordinate of the EE pose. Sample contact probability maps are overlaid on top of the depth images.

## V. EXPERIMENTAL RESULTS

In this section, we present the results of the extrinsic contact estimation problem from the unseen simulation data and in the real world setup to evaluate on sim-to-real transfer. We further explore applications to edge cases such as visual occlusions of the contact and near-contact setups where the active-acoustic signal could provide important cues.

### A. Performance Metrics

We initially assess the model’s capability to classify the binary in-contact or contact-free status of the object-environment interaction. We employ precision, recall, F1, and accuracy scores to compare the performance of our model and ablated models, as summarized in Tab. I.

For the extrinsic contact geometry estimation task, we threshold the probability map output from the model to obtain a binary contact mask and use standard binary mask classification metrics including precision, recall, F1, and accuracy scores. Due to the nature of the contact location or shape evaluation metrics that requires both the ground truth and the predicted masks to be present, we only consider the contact shape or geometry errors for the TP cases.

### B. Simulation Test Results

In Table I, we compare our main model against two baseline models that compares the performance of the three models over 1,400 unseen simulation test cases. The first baseline only uses the current frame’s cropped depth image and the audio input to explore the effects of how much information the audio signals provide about contact events while not using the reference frame and optical flow as input. Another baseline takes the audio modality out from the main model to highlight the effect of having the audio signals along with other modalities. Figure 5 illustrates the various sample contact modes for testing and the respective probability map that is predicted from our model.

Our main model demonstrates good performance across most metrics. For binary contact detection, it achieves the highest F1 score and accuracy, while maintaining a high recall. This indicates that our model not only effectively identifies actual contacts but also minimizes false positives better than the other models. For the contact geometry estimation, our model attains the lowest BCE loss, the highest IOU (0.332), and the lowest Chamfer Distance (3.37 px), reflecting more precise and accurate estimations of contact location and shape. Notably, the model without audio has the highest errors in these metrics, highlighting the importance of audio signals in accurately estimating contact properties.

Interestingly, the depth with audio only baseline performs comparably to the main model and even outperforms the ablated model without audio in these tasks, despite using less visual information. Overall, our proposed model outperforms the baselines, demonstrating the critical role of audio data in accurately detecting and characterizing contact events to complement vision.

### C. Real World Test Results

We evaluate our models on zero-shot sim-to-real transfer capability. Tab. II presents a comparative analysis of our model with and without the audio modality across aforementioned various out-of-distribution real world scenarios S1-S5 to test the role of audio and robustness.

In the *general* case, the model with audio exhibits higher recall and F1 score, indicating a superior ability to detect true contacts. Although the precision is slightly higher without audio (0.734 vs. 0.717), the overall accuracy favors the visual-auditory model (0.694 vs. 0.631). This suggests that audio cues help reduce false negatives without substantially increasing false positives.

Under *occlusion*, the benefits of audio are even more pronounced that the model with audio outperforms the model without audio. Our model with audio achieves a recall of 0.891 compared to 0.522 without audio, and an F1 score of 0.901 versus 0.686. The accuracy also improves significantly (0.82 vs. 0.56). These improvements highlight the model’s enhanced capability to detect contacts that are visually obstructed, leveraging audio cues to compensate for the lack of visual information.

For scenarios involving a *different surface*, both models scores high in binary contact detection metrics. For the contact geometry estimation, the performance of the two models are similar for the model with audio or even better for the model without audio in terms of IOU. This indicates that while our method can transfer to different surface types, which might lead to a variation in audio feedback. The model without audio tends to be less affected by this change as it solely reasons through vision. This indicates that while visual cues are sufficient for high precision, audio input can be generalized across varying surfaces with consistent contact detection.

In the *near contact* scenario, where no ground truth contact masks are available, both models exhibit low accuracy where the model with audio is slightly better. This suggests that detecting near contacts remains challenging, which might be limited by the diversity of real audio data collection compared to the scale of the simulated visual data.

Overall, the integration of audio input into the contact estimation model enhances its ability to reliably detect and localize contacts in complex real-world environments and bridges the sim-to-real transfer well. The audio cues effectively complement visual data, particularly in situations where visual information is incomplete or ambiguous such as under occlusions, which are common in real world manipulation tasks.

Models	Binary Contact Detection				Contact Location, Shape, & Size		
	Precision ( $\uparrow$ )	Recall ( $\uparrow$ )	F1 ( $\uparrow$ )	Acc ( $\uparrow$ )	BCE ( $\downarrow$ )	IOU ( $\uparrow$ )	CD (px)( $\downarrow$ )
Depth + Audio	<b>0.923</b>	<b>0.978</b>	0.923	0.888	0.00432	0.296	3.571
Ours w/o Audio	0.921	0.922	0.921	0.891	0.00475	0.316	4.387
Ours	0.897	0.977	<b>0.935</b>	<b>0.907</b>	<b>0.00399</b>	<b>0.332</b>	<b>3.37</b>

TABLE I: Simulation results of our main model and ablations on 1400 unseen test cases for extrinsic contact prediction. The models are evaluated on binary contact detection and the accuracy of contact geometry estimation, which is only provided for the true positive (TP) cases where the model predicts a mask above a threshold level and the ground-truth is in-contact. CD: Bidirectional Chamfer distance. IOU: Intersection over Union. BCE: Binary cross-entropy loss.

Real World Scenarios (Ours / Ours wo Audio)	Binary Contact Detection				Contact Location, Shape, & Size		
	Precision ( $\uparrow$ )	Recall ( $\uparrow$ )	F1 ( $\uparrow$ )	Acc ( $\uparrow$ )	BCE ( $\downarrow$ )	IOU ( $\uparrow$ )	CD (px) ( $\downarrow$ )
General case	0.717 / <b>0.734</b>	<b>0.929</b> / 0.741	<b>0.809</b> / 0.738	<b>0.694</b> / 0.631	0.0301 / <b>0.0338</b>	0.224 / <b>0.248</b>	<b>11.86</b> / 14.05
Occlusion	0.911 / <b>1.0</b>	<b>0.891</b> / 0.522	<b>0.901</b> / 0.686	<b>0.82</b> / 0.56	<b>0.0316</b> / 0.0433	<b>0.204</b> / 0.0856	<b>12.91</b> / 16.22
Different Surface	<b>1.0</b> / <b>1.0</b>	<b>0.96</b> / 0.90	<b>0.980</b> / 0.947	<b>0.96</b> / 0.9	<b>0.0595</b> / 0.0630	0.293 / <b>0.384</b>	9.984 / <b>5.864</b>
Near Contact	n/a	n/a	n/a	<b>0.12</b> / 0.1	n/a	n/a	n/a

TABLE II: Real world results on extrinsic contact estimation, comparing our model against ours without audio. Note that for the near contact case, there are no ground truth contact mask and therefore some metrics are not applicable (n/a).

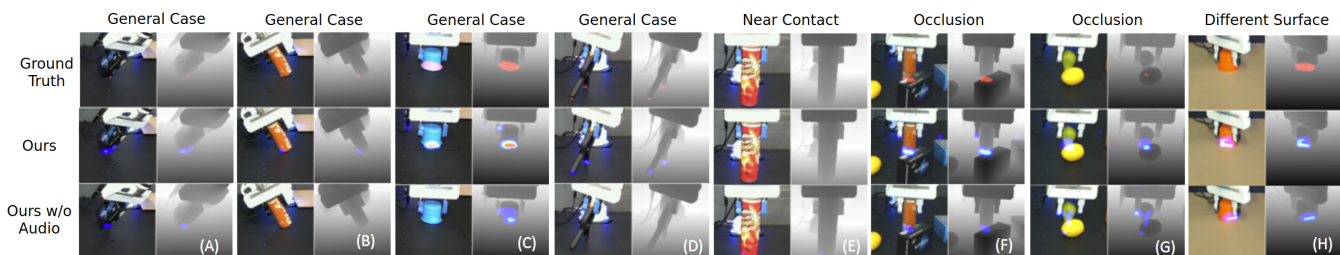


Fig. 6: Zero-shot sim-to-real extrinsic contact predictions on real world scenes (left - RGB, right - Depth). For each case, the ground truth contact masks are plotted in red and the models’ probability map predictions are plotted. (A)-(D) show general cases (S1, S2). (E)-(H) show specific cases (S3, S4, S5).

#### D. Simulation to Real Transfer and Gap

In Fig. 6, we present 8 samples of extrinsic contact estimation on real-world data with different unseen objects. Our model with audio can effectively zero-shot transfer to the real-world scenes under significant perturbations including occlusions from other objects and the presence of audio cables around the gripper that are out-of-distribution from simulated training scenes. For the general cases in Fig. 6(A)-(D), our model with audio can successfully predict point and patch contacts as well as a challenging multi-point contact scene in (D), whereas the model without audio either misses contact points or predicts much smaller contact masks. In Fig. 6(E)-(H), our model predicts visually occluded contacts and near-contact from an actual contact from auditory cues.

## VI. DISCUSSION

We present a real-to-sim audio hallucination and simulation-based method that bridges the sim-to-real gap to estimate extrinsic contacts using multimodal signals from active-audio sensing at the fingertips, vision, and proprioception. This study demonstrates the potential of active-audio sensing to provide valuable local information about contact events and to complement vision for robotic manipulation.

However, several areas for improvement remain in audio representations, system design, and diversity of real-world audio signals in data collection. Exploring alternative audio representations could improve the efficiency and accuracy of

feature extraction. Additionally, integrating large pretrained audio models could provide more comprehensive features.

Our object selection was limited to rigid or slightly deformable objects with low vibration absorption to focus on clean audio data. Expanding to softer, deformable objects introduces greater complexity due to their higher and more variable absorption rates, but doing so is crucial for broader applicability. Additionally, challenges in annotating contact masks and collecting real-world audio data constrained our dataset size. Addressing these challenges will be necessary to make the system more robust and generalizable.

We focused on direct extrinsic contacts, but future work could explore chains of contact events. These scenarios, where signals pass through multiple contacts, lead to higher audio signal loss, necessitates systems with higher signal-to-noise ratio (SNR). A key challenge we faced is the internal noise generated by the robot’s vibrations, which was more significant than airborne noise. The vibrations in the Franka gripper during object manipulation lowered the SNR. Future designs should also focus on improving vibration isolation in the robotic finger to mitigate noise and enhance SNR.

Regarding the vibration source, we chose a conductive speaker over a vibration motor due to its integration with off-the-shelf libraries and ease of implementation. However, vibration motors, with their stronger vibrations, offer potential for future use as actuators, presenting an interesting direction for further research.

## REFERENCES

- [1] Leon Kim, Yunshuang Li, Michael Posa, and Dinesh Jayaraman. Im2contact: Vision-based contact localization without touch or force sensing. In *Conference on Robot Learning*, pages 1533–1546. PMLR, 2023.
- [2] Alessandro De Luca, Alin Albu-Schaffer, Sami Haddadin, and Gerd Hirzinger. Collision detection and safe reaction with the dlr-iii lightweight manipulator arm. In *2006 IEEE/RSJ International Conference on Intelligent Robots and Systems*, pages 1623–1630. IEEE, 2006.
- [3] Lucas Manuelli and Russ Tedrake. Localizing external contact using proprioceptive sensors: The contact particle filter. In *2016 IEEE/RSJ International Conference on Intelligent Robots and Systems (IROS)*, pages 5062–5069. IEEE, 2016.
- [4] Antonio Bicchi, J Kenneth Salisbury, and David L Brock. Contact sensing from force measurements. *The International Journal of Robotics Research*, 12(3):249–262, 1993.
- [5] Carolina Higuera, Siyuan Dong, Byron Boots, and Mustafa Mukadam. Neural contact fields: Tracking extrinsic contact with tactile sensing. In *2023 IEEE International Conference on Robotics and Automation (ICRA)*, pages 12576–12582. IEEE, 2023.
- [6] Kuan-Ting Yu and Alberto Rodriguez. Realtime state estimation with tactile and visual sensing for inserting a suction-held object. In *2018 IEEE/RSJ International Conference on Intelligent Robots and Systems (IROS)*, pages 1628–1635. IEEE, 2018.
- [7] Daolin Ma, Siyuan Dong, and Alberto Rodriguez. Extrinsic contact sensing with relative-motion tracking from distributed tactile measurements. In *2021 IEEE international conference on robotics and automation (ICRA)*, pages 11262–11268. IEEE, 2021.
- [8] Sangwoon Kim, Devesh K Jha, Diego Romeres, Parag Patre, and Alberto Rodriguez. Simultaneous tactile estimation and control of extrinsic contact. In *2023 IEEE International Conference on Robotics and Automation (ICRA)*, pages 12563–12569. IEEE, 2023.
- [9] Andrea Sipos and Nima Fazeli. Simultaneous contact location and object pose estimation using proprioception and tactile feedback. In *2022 IEEE/RSJ International Conference on Intelligent Robots and Systems (IROS)*, pages 3233–3240. IEEE, 2022.
- [10] Andrea Sipos and Nima Fazeli. Multiscope: Disambiguating in-hand object poses with proprioception and tactile feedback. *arXiv preprint arXiv:2305.14204*, 2023.
- [11] Sangwoon Kim and Alberto Rodriguez. Active extrinsic contact sensing: Application to general peg-in-hole insertion. In *2022 International Conference on Robotics and Automation (ICRA)*, pages 10241–10247. IEEE, 2022.
- [12] Chris Harrison and Scott E Hudson. Scratch input: creating large, inexpensive, unpowered and mobile finger input surfaces. In *Proceedings of the 21st annual ACM symposium on User interface software and technology*, pages 205–208, 2008.
- [13] Shihan Lu, Yang Chen, and Heather Culbertson. Towards multisensory perception: Modeling and rendering sounds of tool-surface interactions. *IEEE transactions on haptics*, 13(1):94–101, 2020.
- [14] Abitha Thankaraj and Lerrel Pinto. That sounds right: Auditory self-supervision for dynamic robot manipulation. In *Conference on Robot Learning*, pages 1036–1049. PMLR, 2023.
- [15] Hao Li, Yizhi Zhang, Junzhe Zhu, Shaoxiong Wang, Michelle A Lee, Huazhe Xu, Edward Adelson, Li Fei-Fei, Ruohan Gao, and Jiajun Wu. See, hear, and feel: Smart sensory fusion for robotic manipulation. *arXiv preprint arXiv:2212.03858*, 2022.
- [16] Jared Mejia, Victoria Dean, Tess Hellebrekers, and Abhinav Gupta. Hearing touch: Audio-visual pretraining for contact-rich manipulation. *arXiv preprint arXiv:2405.08576*, 2024.
- [17] Gabriel Zöllner, Vincent Wall, and Oliver Brock. Acoustic sensing for soft pneumatic actuators. In *2018 IEEE/RSJ International Conference on Intelligent Robots and Systems (IROS)*, pages 6986–6991. IEEE, 2018.
- [18] Ken Takaki, Yoshitaka Taguchi, Satoshi Nishikawa, Ryuma Niiyama, and Yoshihiro Kawahara. Acoustic length sensor for soft extensible pneumatic actuators with a frequency characteristics model. *IEEE Robotics and Automation Letters*, 4(4):4292–4297, 2019.
- [19] Gabriel Zöllner, Vincent Wall, and Oliver Brock. Active acoustic contact sensing for soft pneumatic actuators. In *2020 IEEE International Conference on Robotics and Automation (ICRA)*, pages 7966–7972. IEEE, 2020.
- [20] Shinichi Mikogai, BDC Kazumi, and Kentaro Takemura. Contact point estimation along air tube based on acoustic sensing of pneumatic system noise. *IEEE Robotics and Automation Letters*, 5(3):4618–4625, 2020.
- [21] Uksang Yoo, Ziven Lopez, Jeffrey Ichnowski, and Jean Oh. Poe: Acoustic soft robotic proprioception for omnidirectional end-effectors. *arXiv preprint arXiv:2401.09382*, 2024.
- [22] Xiaoran Fan, Riley Simmons-Eidler, Daewon Lee, Larry Jackel, Richard Howard, and Daniel Lee. Aurasense: Robot collision avoidance by full surface proximity detection, 2021.
- [23] Shihan Lu and Heather Culbertson. Active acoustic sensing for robot manipulation. In *2023 IEEE/RSJ International Conference on Intelligent Robots and Systems (IROS)*, pages 3161–3168. IEEE, 2023.
- [24] Maximilian Du, Olivia Y Lee, Suraj Nair, and Chelsea Finn. Play it by ear: Learning skills amidst occlusion through audio-visual imitation learning. *arXiv preprint arXiv:2205.14850*, 2022.
- [25] Zachary Teed and Jia Deng. Raft: Recurrent all-pairs field transforms for optical flow, 2020.
- [26] Viktor Makoviychuk, Lukasz Wawrzyniak, Yunrong Guo, Michelle Lu, Kier Storey, Miles Macklin, David Hoeller, Nikita Rudin, Arthur Allshire, Ankur Handa, and Gavriel State. Isaac gym: High performance gpu-based physics simulation for robot learning, 2021.
- [27] Berk Calli, Arjun Singh, Aaron Walsman, Siddhartha Srinivasa, Pieter Abbeel, and Aaron M Dollar. The ycb object and model set: Towards common benchmarks for manipulation research. In *2015 international conference on advanced robotics (ICAR)*, pages 510–517. IEEE, 2015.
- [28] Olaf Ronneberger, Philipp Fischer, and Thomas Brox. U-net: Convolutional networks for biomedical image segmentation. In *Medical image computing and computer-assisted intervention—MICCAI 2015: 18th international conference, Munich, Germany, October 5-9, 2015, proceedings, part III 18*, pages 234–241. Springer, 2015.
- [29] Rosanne Liu, Joel Lehman, Piero Molino, Felipe Petroski Such, Eric Frank, Alex Sergeev, and Jason Yosinski. An intriguing failing of convolutional neural networks and the coordconv solution, 2018.
- [30] Lihe Yang, Bingyi Kang, Zilong Huang, Xiaogang Xu, Jiashi Feng, and Hengshuang Zhao. Depth anything: Unleashing the power of large-scale unlabeled data. In *CVPR*, 2024.